PFC/JA-86-3

Design and Performance of Compact Vacuum-Compatible Submillimeter Viewing Dumps

K. Kato and I. H. Hutchinson

Plasma Fusion Center
Massachusetts Institute of Technology
Cambridge, MA 02139

January 1986

This work was supported by the U.S. Department of Energy Contract No. DE-AC02-78ET51013. Reproduction, translation, publication, use and disposal, in whole or in part by or for the United States government is permitted.

Submitted to: Review of Scientific Instruments

Design and Performance of Compact Vacuum-Compatible Submillimeter Viewing Dumps

K. Kato and I. H. Hutchinson

Plasma Fusion Center, Massachusetts Institute of Technology

Cambridge, Massachusetts, 02139, U.S.A.

ABSTRACT

Compact, vacuum-compatible submillimeter viewing dumps, whose design parameters were based on the results of simple ray calculations, have been fabricated from Pyrex, Macor, and alumina. The measured performance of the dumps agrees qualitatively with calculated results. The absorption is somewhat lower than expected, but still acceptable($\geq$ 99% absorption for Pyrex and Macor). In an electron cyclotron plasma emission experiment on Alcator C tokamak, comparison of the emission spectra with and without the dump shows that the dump in this configuration is effective in supressing the unwanted radiation by approximately 90%. The additional reflection is believed to be due to a portion of the antenna pattern missing the dump.

INTRODUCTION

Vacuum compatible viewing dumps that absorb electromagnetic radiation in the far infrared and millimeter wavelengths are required in plasma experiments such as electron density profile measurements using ECE(electron cyclotron emission)[1], and ion temperature measurements using FIR Thomson scattering[2]. Without viewing dumps, these measurements are severely contaminated by reflections off the metallic walls. In this paper, the design and performance of submillimeter viewing dumps constructed for an ECE experiment on Alcator C tokamak[3] is discussed. A simple approach of using an eccosorb screen, for example, is not satisfactory for this purpose since the dump must be compatible with the high vacuum and the high temperature environment of the plasma confinement vessel.

In the past, dumps made of graphite have been used at $385\mu m(780GHz)$ for Thomson scattering in Alcator C[4], but with little success owing to graphite's relatively high reflectivity. Eccosorb filled glass capsules have been used at frequencies below $30GHz$, providing increase in measured polarization of ECE from the Tokapole device[5]. The requirements for dumps discussed here include high absorptivity in the wide frequency range of $100GHz$ to $1000GHz$ and plasma compatibility.

I. DESIGN AND FABRICATION

An absorptivity of greater than 99% is used as the design goal of the dumps for the ECE diagnostic. A spatial constraint, arising from the small access and limited space in Alcator C[6] limits the size of the dump(especially the thickness)

to $7cm \times 7cm \times 1cm$. For design purposes, two assumptions are made. They are; (1) the dump material is chosen to have a large absorption coefficient although still with the real part of the refractive index much greater than the imaginary part, and (2) geometrical optics is valid. The first assumption allows us to consider the fraction of the ray which is transmitted into the material to be completely absorbed. The second assumption allows us to execute simple ray-tracing to plot the ray trajectory. The ray's angle of incidence obtained in this way enables the calculation of the transmitted and the reflected electric field components for a given wave polarization and the refractive index of the material. These relations are given by[7],

$$\begin{aligned}
\left(\frac{E_r}{E_i}\right)_{\|} &= \frac{(N_2/N_1)^2\cos\theta - \sqrt{(N_2/N_1)^2 - \sin^2\theta}}{(N_2/N_1)^2\cos\theta + \sqrt{(N_2/N_1)^2 - \sin^2\theta}} \\
\left(\frac{E_r}{E_i}\right)_{\perp} &= -\frac{\cos\theta - \sqrt{(N_2/N_1)^2 - \sin^2\theta}}{\cos\theta + \sqrt{(N_2/N_1)^2 - \sin^2\theta}} \\
\left(\frac{E_t}{E_i}\right)_{\|} &= \frac{N_1}{N_2}\left(1 + \left(\frac{E_r}{E_i}\right)_{\|}\right) \\
\left(\frac{E_t}{E_i}\right)_{\perp} &= 1 - \left(\frac{E_r}{E_i}\right)_{\perp},
\end{aligned} \tag{1}$$

where E is the electric field, N is the refractive index(here assumed to be purely real), $r, t,$ and i refer to reflected, transmitted, and incident rays, respectively, and 1 and 2 refer to the different dielectric media. Polarizations, parallel($\|$) and perpendicular($\perp$), are defined with respect to the plane of incidence. The symbols and geometries used in the above equations are defined in Fig.1. In general, parallel polarization is reflected less, throughout most of the range of angles of incidence.

The above two assumptions are at best crude. The assumption of large absorptivity breaks down when the thickness of the dump is small compared to the

reciprocal of the absorption coefficient. In this case, a fraction of the transmitted ray can reemerge, contributing to the reflected power. The second assumption of geometrical optics breaks down when the dimensions of the viewing dump structure becomes comparable to the wavelength. Hence, both of these assumptions tend to underestimate the reflectivity for dumps of size comparable to the inverse absorption coefficient, or the wavelength, respectively.

Shapes often used for viewing dumps include conic structure, pyramid arrays, an array of horns, or straight grooves. These all have the effect of increasing absorption by inducing multiple reflections. The first three shapes are difficult to fabricate, but the reflectivity is independent of the relative orientation of the dump and the polarization vector. On the other hand, a groove structure is somewhat easier to make, but is sensitive to the polarization. The shape of the dumps discussed here is the straight groove structure, selected primarily for its ease in fabrication.

In general, the relationship between k, the number of front surface reflections before the ray reemerges from the groove, and θ_g, the groove angle can be written,

$$k = \frac{\pi}{\theta_g}, \tag{2}$$

for a ray normally incident on the dump. A fractional k indicates that the ray eventually emerges non-normal to the dump. This relationship arises as a simple consequence of ray tracing, and is illustrated in Fig.2, using real space(a), and semi-circle representation(b). The groove angle shown here is 45^o.

Three candidate materials are selected, which have both good vacuum properties and absorption properties. They are Pyrex, Macor[8], and alumina. All three materials are compatible with the Alcator vacuum($10^{-9}Torr$), with low reflectivity and high absorption coefficient. Table I shows the refractive indicies for these materials. The absorption coefficient, $\alpha(cm^{-1})$, at $400GHz$ for Pyrex, Macor, and

alumina are 6.2[9], 5.1, and 0.41[10], respectively. From this data, Pyrex is expected to provide the best performance, followed by Macor, then alumina. Both Macor and alumina can withstand temperatures in excess of 1000^oC. Pyrex has a softening point temperature of approximately 800^oC.

Also shown in Table I are the front surface reflectivities computed using Eq.(1) for Pyrex, Macor, and alumina for normally incident rays and for various groove angles. The values indicate that for Pyrex and Macor, the design goal of 99% absorption can be achieved with a groove angle of 45^o or with four reflections. The requirement becomes more critical for alumina, which requires an angle of 30^o. In all cases, it is seen that parallel polarized waves have much lower front surface reflectivity.

In spite of the calculated results of Table I, all three dumps were made with the 45^o groove angle, so the alumina dump is not expected to fulfill the design goal. The size of the dump structure was determined such that the groove spacing is $5mm$ and the depth is $6mm$. There is also a $4mm$ thick substrate of the same material. The schematic of the dump with dimensions is shown in Fig.3(a). While it was possible to make this out of one piece of Macor by machining, Pyrex and alumina, which had to be ground, were made of many identical groove pieces as shown in Fig.3(b)[11]. The pieces were then placed together to form the entire dump. The lip along the perimeter is used to hold the dump in place.

II. PERFORMANCE

The performance of the dumps was evaluated in the frequency range $100GHz$ to $1000GHz$. The measurement configuration is shown in Fig.4. A mercury arc

lamp[12] with a chopper is used as the broad band source, and the reflected signal is detected by the InSb detector connected to a lock-in amplifier. The spectral response of the mercury arc lamp—InSb detector system is ideally matched to the frequency range of interest, with the peak of the spectrum at $550GHz$ and FWHM of $700GHz$[13]. To minimize the angle subtended by the source and the detector, a copper waveguide extension was attached to the detector, placing it behind the source. In this way, a minimum angle of 20^o between the source and the detector is achieved while still ensuring that the detector only see the dump surface. For polarization measurements, fine wire grid polarizers were placed in front of the source. The sample dump was held in place by an aluminum frame covered with eccosorb microwave absorber. The angular spread of the reflected radiation is obtained by scanning the detector in a circular path about the dump.

Both polarized and unpolarized radiation were used as the source. In addition, since the detector can only be scanned in the plane of the table, measurements were taken for the two orientations of the groove, vertical and horizontal(Fig.4 shows the dump in vertical orientation). A measurement with a stainless steel slab placed in the dump frame is used for reflected power normalization.

Table II shows the results of specular reflection measurement for the three polarizations; unpolarized, electric field vector parallel to the plane of incidence, and perpendicular to the plane of incidence(See Fig.1). (H) and (V) after the dump material indicate horizontal and vertical orientation, respectively. All measurements are normalized to the specularly reflected power of the stainless steel slab(= 100). Measured values indicate higher absorption for the parallel polarization in general, in qualitative agreement with results of Table I. The ordering of the effectiveness also agrees with the calculations. Pyrex is found to be the most effective, with Macor slightly worse, and alumina being the worst of the three. However, the quantitative

agreement is only approximate for the perpendicular polarization, and is off by orders of magnitude for the parallel polarization. We believe these discrepancies are due to incomplete absorption of the transmitted power in the body of the dump, and may therefore be reduced in a thicker dump. Note that the specular reflectivity value for a given dump depends on the groove orientation. The horizontal orientation always gives larger values. In subsequent text, the angular measurements obtained with the grooves horizontal is referred to as the H-scan while the spectra with grooves oriented vertical is referred to as the V-scan.

Fig.5 shows the reflected power as a function of the detector angle measured from the specular position for unpolarized radiation. The V-scan shows a relatively low peak and a wide tail, extending to large angles. The cause of this wide tail is believed to be low frequency($f \lesssim 250GHz$) waves diffracting off the dump grooves, and internal reflections within the dump giving rise to waves reemerging in random directions. The H-scan shows a relatively high peak with narrow width, extending approximately to 15^o. The shapes of the profiles for a given dump orientation are quite similar for all materials and polarizations. Measurements with the polarized source produce similar spectra, shifted up or down by the relative value of reflection at the specular angle.

The difference in the specularly reflected power for different groove orientations is accounted for mainly by the retrospecular nature of the front surface reflected rays. As an example, the ray shown by a dashed line in Fig.2(a) enters the groove at 10^o to the normal and exits it parallel to the original ray. Thus, in the V-scan, these retro-specular reflections do not get detected, and a lower value for reflected power results.

Therefore, to obtain the aggregate reflection spectra over the hemisphere facing the detector, a rather simple approach is taken, of adding the retrospecular power

component to the V-scan so as to make the peak value at normal reflection equal, as shown schematically in Fig.6. Insofar as the angular distribution of reflected power can be approximated as a retrospecular peak plus other broader features, this will provide a reasonable estimate, regardless of the exact cause of the broader scattering. The total angular distribution is then taken to be the product of separate angular functions in the horizontal and vertical directions, $I(\theta_H, \theta_V) = f_H(\theta_H) f_V(\theta_V)$. Thus the total reflected power is given by

$$\begin{aligned} P_R &= \int_{-\pi/2}^{\pi/2} \int_{-\pi/2}^{\pi/2} I(\theta_H, \theta_V) d\theta_H \cos\theta_V d\theta_V \\ &= \int_{-\pi/2}^{\pi/2} f_H(\theta_H) d\theta_H \int_{-\pi/2}^{\pi/2} f_V(\theta_V) \cos\theta_V d\theta_V, \end{aligned} \tag{3}$$

where P_R is the total reflected power. For the purpose of this integration, orthogonal detector angles from the normal, θ_H and θ_V, are assumed similar to spherical coordinate variables, θ(the polar angle) and ϕ(the azimuthal angle), with $\theta_H = \phi$ and $\theta_V = \pi/2 - \theta$. Negligible error is introduced since most of the reflected power is concentrated near $\theta_H \simeq \theta_V \simeq 0$. Nevertheless, θ_V, with its greater angular spread, is associated with the polar angle to bring out the spherical dependence. By comparing this with the total reflected power from a stainless steel slab, the absorption by the dump is obtained. Results are summarized in Table III. It shows that the design goal of less than 1% reflection is achieved with the Pyrex dump regardless of the source polarization. The goal is also achieved for parallel polarization with the Macor dump, but alumina dump is noticeably worse.

The spectral response of the dump was measured using the mercury arc lamp source and a rapidly-scanning Michelson interferometer[14] in place of the broad band detector. This is a particularly difficult and time consuming measurement since the level of the mercury arc radiation reflected off the dump is equivalent to

that of a $T \lesssim 30K$ blackbody. A single measurement was made for the Macor dump, in the H-scan orientation for the parallel polarization. The normalized reflected power curve, measured by co-addition of more than 40,000 interferograms, is shown by a broken line in Fig.7. Further attempt to reduce the noise appears impractical. The smoothed approximation indicated by the solid line shows less absorption at the low frequency end where geometrical optics breaks down and the absorption coefficient is lower. Small amplitude features of the smoothed curve at higher frequencies are probably not statistically significant. This inferior performance at low frequency is also supported by a separate measurement using a low pass filter at the broad band detector aperture. The frequency integrated response, appropriately weighted by the source spectrum, is in fair agreement with the value shown in Table II.

III. APPLICATION

These dumps were fabricated as a part of the vertical viewing ECE experiment, the purpose of which is to isolate the region of ECE to a narrow chord to measure the electron velocity distribution[15]. The measurement requires a specialized optical arrangement, as well as the viewing dump at the termination point.

The configuration of the experiment is shown schematically in Fig.8. The Pyrex or Macor dump was placed at the bottom of the tokamak torus, surrounded by a stainless steel frame to provide additional protection from the plasma particles. The distance between the tip of the grooves and the limiter-defined plasma edge is approximately $1.5cm$. Three front surface mirrors were used to image the plasma onto the Michelson interferometer aperture.

Second harmonic ECE profiles from thermal plasmas at a magnetic field of $8Tesla$ were used for the performance analysis in the range $380GHz \leq f \leq 560GHz$. These profiles, selected for their reproducibility, were taken with and without the Macor dump, and for ordinary and extraordinary modes of propagation($E \parallel B_T$ and $E \perp B_T$, respectively). They are shown in Fig.9. The dump grooves were oriented parallel to the toroidal field, so that attenuation of extraordinary mode emission is favored.

Without the dump, emission from essentially the entire plasma diameter($33cm$) is observed because the intensity is dominated by the multiple passes of reflected rays through the plasma. The emission with the dumps has dramatically decreased width, corresponding to about $3cm$ in the major radius direction for the FWHM. This is consistent with the calculations of beam width at the plasma center, so that most of the radiation is coming from within the line of sight.

The comparison of the emission levels from outside the line of sight shows that the optical arrangement is effective in reducing the reflected emission by $\geq 90\%$. This discrepancy in performance is believed to be due to a portion of the antenna pattern missing the dump and accepting reflections off the frame, even though the antenna pattern width at the dump was minimized consistent with the other optical requirements.

The Pyrex dump was found to have cracked at the groove tips (apparently because of thermal shocks) after three weeks($\simeq$ 1000 plasma discharges, $t = 0.5sec/$ discharge). There was no structural damage to the Macor dump(also after three weeks). No obvious performance degradation from either dump was observed during this period, despite metal particle deposits on the surface. Furthermore, no additional plasma impurity problems caused by the dump were observed, despite its close proximity to the plasma.

In summary, we have fabricated and tested submillimeter viewing dumps made of Pyrex, Macor, and alumina. A simple front surface reflectivity calculation provides a fair estimate of their performance, which, for Pyrex and Macor, is $\geq 99\%$ absorption of the incident radiation. Use of these dumps in a plasma ECE experiment has resulted in a dramatic reduction of multiple reflections.

ACKNOWLEDGEMENTS

The authors gratefully acknowledge Dr. Woskoboinikow for many helpful discussions and advice, especially with respect to the initial selection of the candidate dump materials. Many thanks go to Drs. Gandy and Gomez for helpful suggestions on the performance tests, and to the rest of the Alcator Group for their support. This work was supported by Department of Energy contract DE-AC02-78ET51013.

REFERENCES

[1] F. Engelmann and M. Curatolo, Nucl. Fusion, 13(1973)497.

[2] P. Woskoboinikow, H.C. Praddaude, W.J. Mulligan, D.R. Cohn, B. Lax, and H.R. Fetterman, 6th Int. Conf. Infrared and Millimeter Waves, Conf. Digest, IEEE Cat. No. 81 CH1645-1 MTT(1981) M-3-1.

[3] K. Kato and I.H. Hutchinson, Bull. Am. Phys. Soc. Vol.29, No.8, p.1223 (Oct. 1984).

[4] P. Woskoboinikow, R. Erickson and W.J. Mulligan, Int. J. Infrared and Millimeter Waves, Vol.4, p.1045(1983).

[5] M.A. Sengstacke, R.N. Dexter, and S.C. Prager, Phys. Fluids, 28(1985)403.

[6] C. Weggel, W. Hamburger, B. Montgomery, and N. Pierce, Proc. 7th Symposium on Engineering Problems of Fusion Research, p.54, Knoxville, Tennessee, 1977.

[7] G. Bekefi and A. Barrett, *Electromagnetic Vibrations, Waves, and Radiation,* MIT Press, Cambridge, Mass. 1977.

[8] V.O. Altemose and A.R. Kacyon, "Vacuum Compatibility of Machinable Glass Ceramics," Corning Tech. Paper, Corning Glass Works, Corning, N.Y.

[9] K.H. Breeden and A.P. Sheppard, Radio Science, 3 (1968) 205.

[10] M.N. Afsar and K.J. Button, IEEE Transactions on Microwave Theory and Techniques, Vol.MTT-31, No.2, Feb. 1983.

[11] Grinding of dump pieces were done at Ceramic Grinding Company, Waltham, MA.

[12] M.F. Kimmit, *Far Infrared Techniques,* Pion (1970).

[13] I.H. Hutchinson and S.E. Kissel, Proc. 4th Int. Conf. Infrared and Millimeter Waves and their Applications, p.76, Miami Beach, 1979.

[14] D.H. Martin and E. Puplett, Infrared Phys. 10 (1970) 105.

[15] I.H. Hutchinson and K. Kato, "Diagnosis of Mildly Relativistic Electron Distributions by Cyclotron Emission," PFC/JA-85-15, to be published in Nucl. Fusion.

FIGURE CAPTIONS

Fig.1. Notation of field vectors at a dielectric interface, used in Eq.(1).

Fig.2. (a) Path of a normally incident ray through a 45^o groove in real space(solid line). The path of a ray incident at 10^o to normal is shown by the dashed line.

(b) Path of a normally incident ray through a 45^o groove in semi-circle representation. The groove is duplicated and spread into a semi-circle so that the path of the ray is shown by a straight line.

Fig.3. (a) Dimensions of the viewing dumps. (b) Modular construction of the Pyrex and the Alumina dumps.

Fig.4. Measurement configuration as viewed from above(not to scale).

Fig.5. Reflected power from different dumps as a function of the detector angle. (Noise level $\simeq 5 \times 10^{-3} A.U.$)

Fig.6. Schematic picture of the normal incidence approximation. The angular distribution of the reflected power, I, is plotted as a function of the two orthobonal orientations, θ_H for the H-scan, and θ_V for the V-scan.

Fig.7. Frequency response of the Macor dump at 10^{o} specular orientation, with grooves oriented in the H-scan direction and for parallel polarization. Broken line shows the measured spectrum. Solid line is the smoothed approximation.

Fig.8. Experiment configuration of the Vertical Viewing ECE diagnostic.

Fig.9. Second harmonic ECE spectrum from Alcator C plasma $n_e \simeq 1.7 \times 10^{20} m^{-3}, 350kA \leq I_p \leq 400kA, B_T = 8Tesla$. Trace A. Extraordinary mode, without the dump; Trace B. ordinary mode, without the dump; Trace C. extraordinary mode, with the dump; Trace D. ordinary mode, with the dump.

TABLE I. Refractive indicies and computed reflectivities for different materials. Reflectivities are computed for the parallel and perpendicular electric field orientation. (Values are normalized to incident power of unity.)

–	Polarization	Pyrex	Macor	Alumina
N	–	2.1[i]	2.4[ii]	3.1[ii]
$\theta_g = \pi/3$	$\parallel$	3×10^{-6}	4×10^{-5}	8×10^{-4}
$\pi/3$	$\perp$	0.02	0.03	0.07
$\pi/4$	$\parallel$	1×10^{-7}	8×10^{-13}	8×10^{-6}
$\pi/4$	$\perp$	0.004	0.01	0.03
$\pi/6$	$\parallel$	1×10^{-7}	2×10^{-7}	7×10^{-8}
$\pi/6$	$\perp$	3×10^{-4}	0.001	0.006

[i] From Ref.9.

[ii] From Ref.10.

TABLE II. Measured specular reflectivity(%) at 10° incidence angle.

Dump	Unpolarized	$\perp$	$\parallel$
S.S.	100	100	100
Pyrex(H)	0.32	0.46	0.17
Pyrex(V)	0.074	0.079	0.060
Macor(H)	0.58	0.91	0.23
Macor(V)	0.13	0.12	0.12
Alumina(H)	4.2	4.3	3.8
Alumina(V)	1.3	1.2	1.4

TABLE III. Angle integrated total measured reflection(%).

Polarization	Pyrex	Macor	Alumina
Unpolarized	0.63	0.98	7.3
$\perp$	0.87	1.5	7.3
$\parallel$	0.40	0.45	6.8

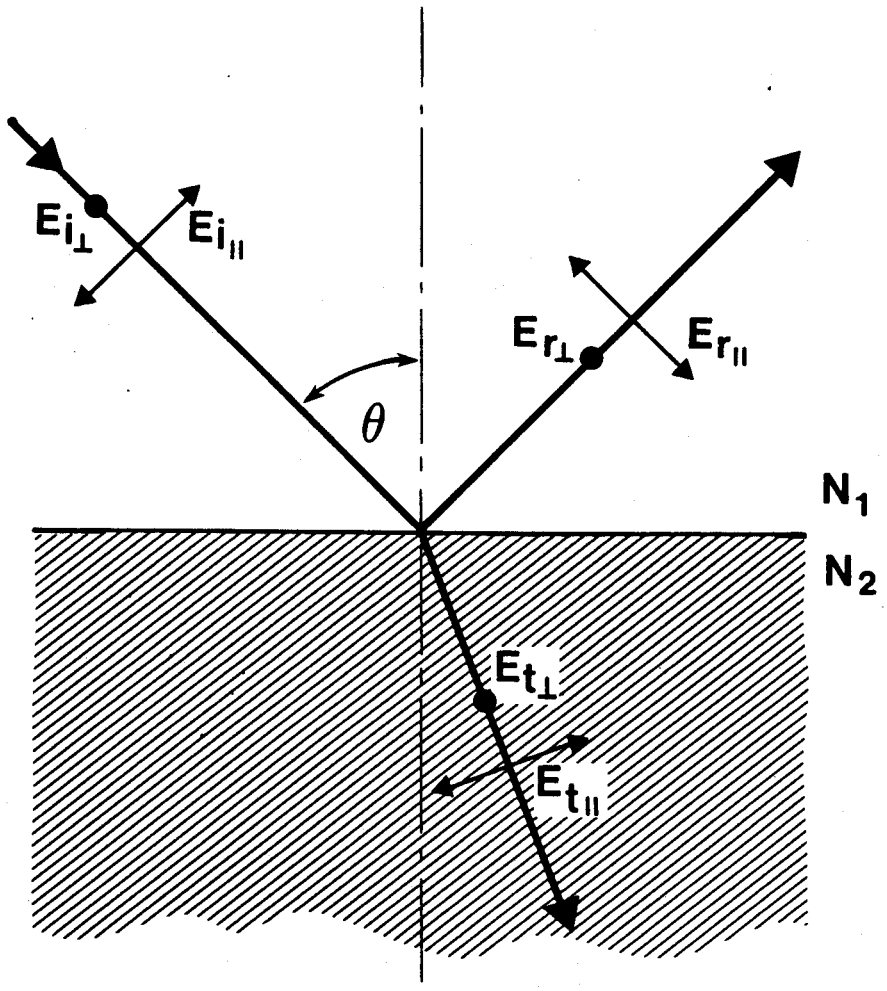
$E_{i\perp}$
$E_{i\parallel}$
$E_{r\perp}$
$E_{r\parallel}$
θ
N_1
N_2
$E_{t\perp}$
$E_{t\parallel}$

Figure 1.

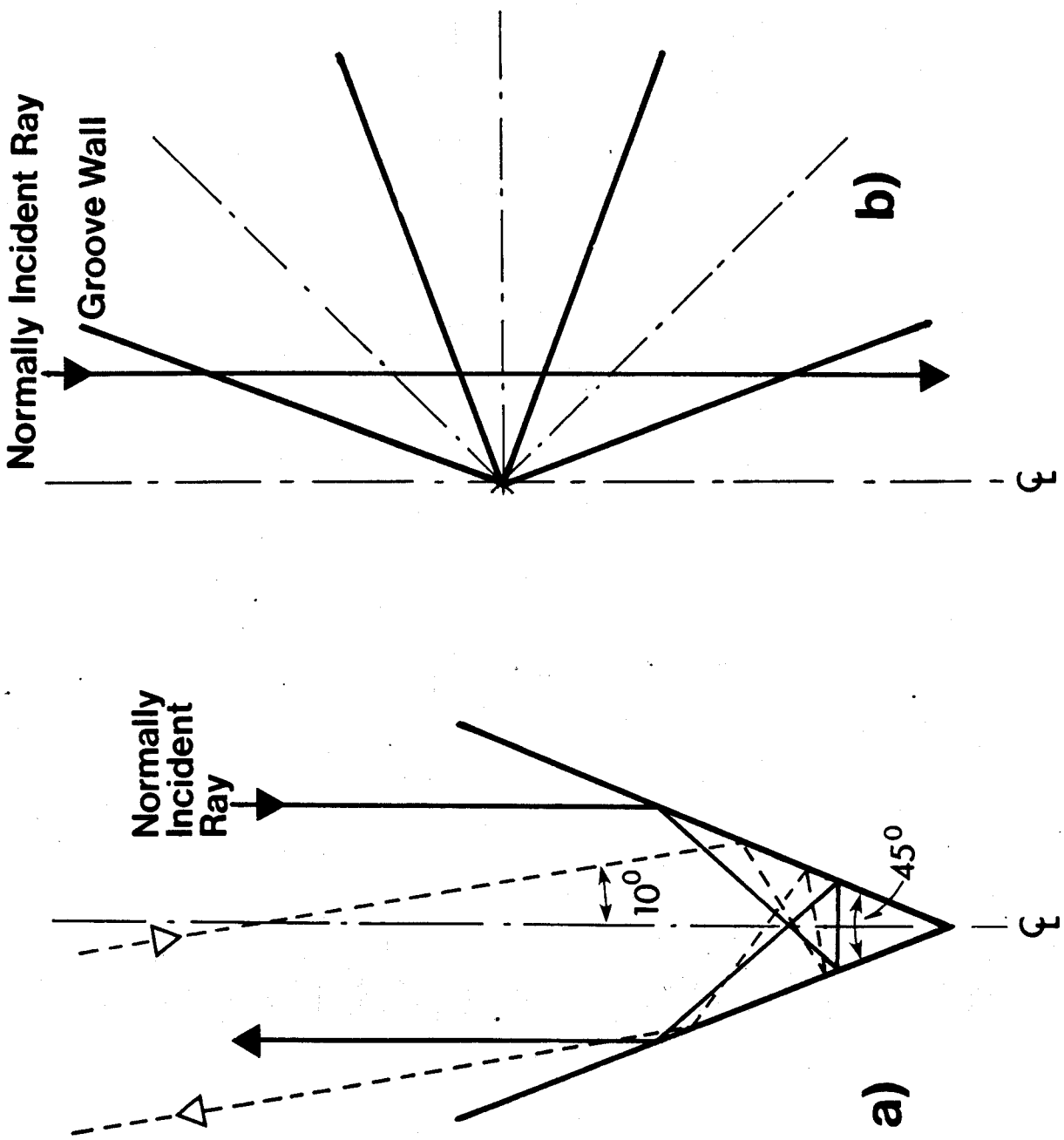
Normally Incident Ray
Groove Wall
b)
ξ
Normally Incident Ray
10°
45°
ξ
a)

Figure 2.

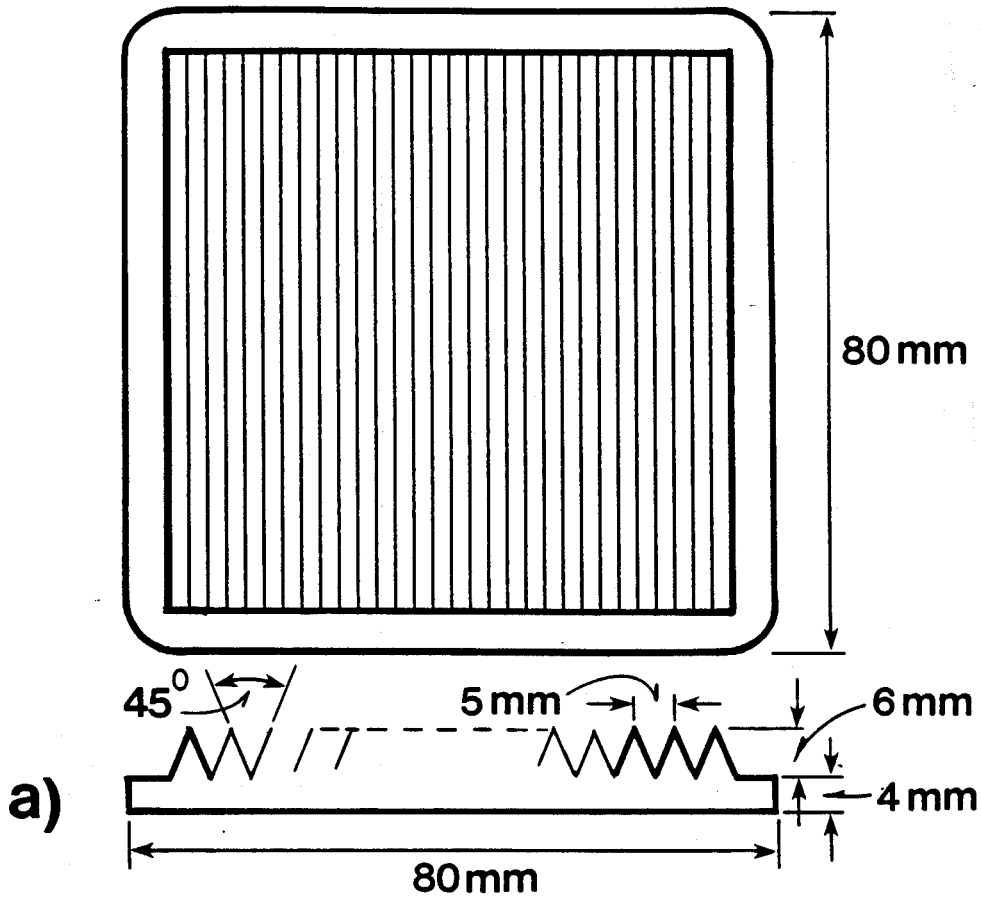

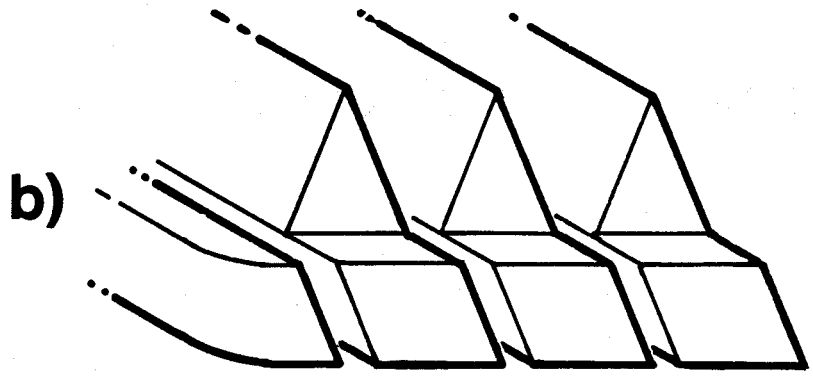

Figure 3.

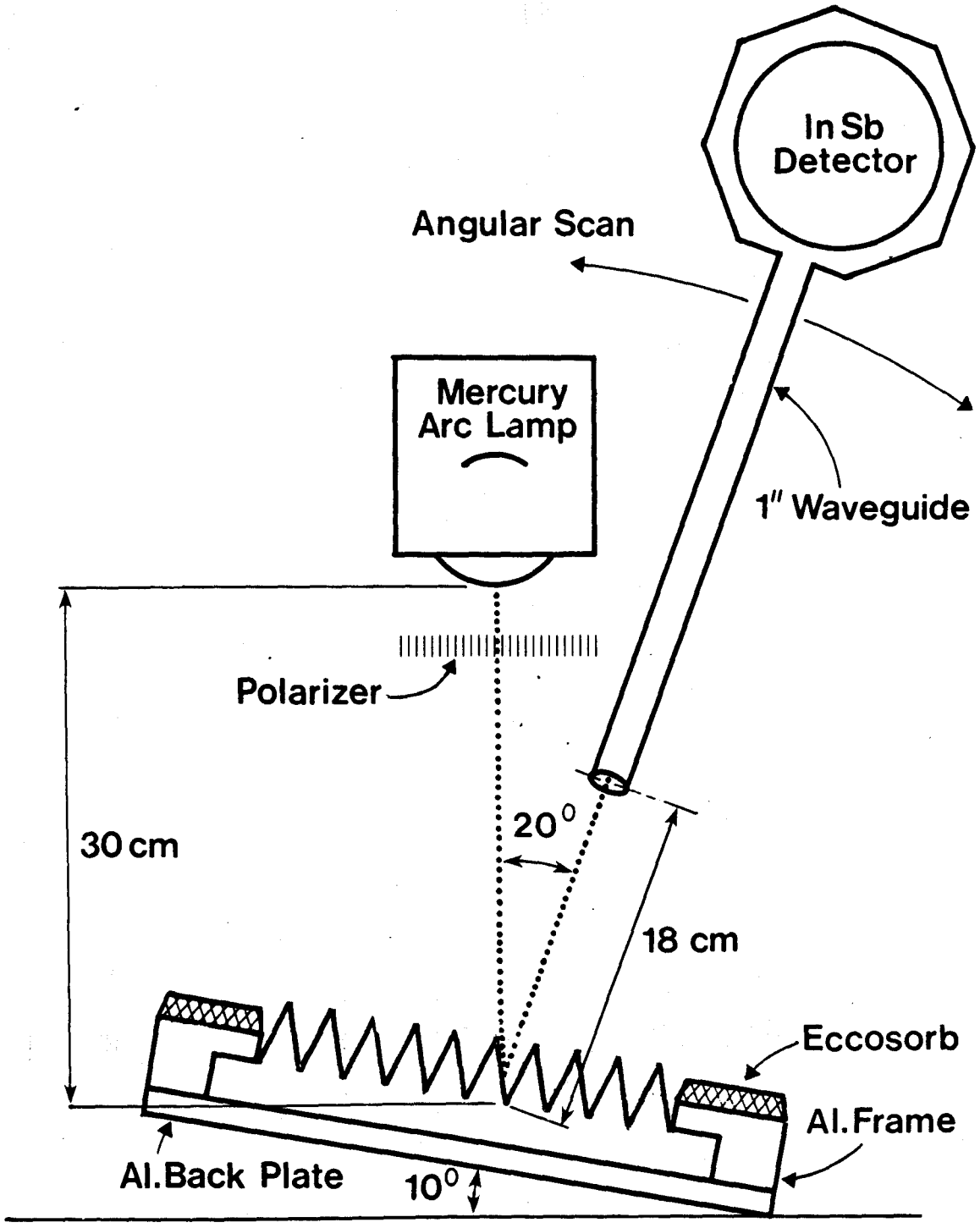
In Sb
Detector
Angular Scan
Mercury
Arc Lamp
1" Waveguide
Polarizer
30 cm
20°
18 cm
Eccosorb
Al. Frame
Al. Back Plate
10°

Figure 4.

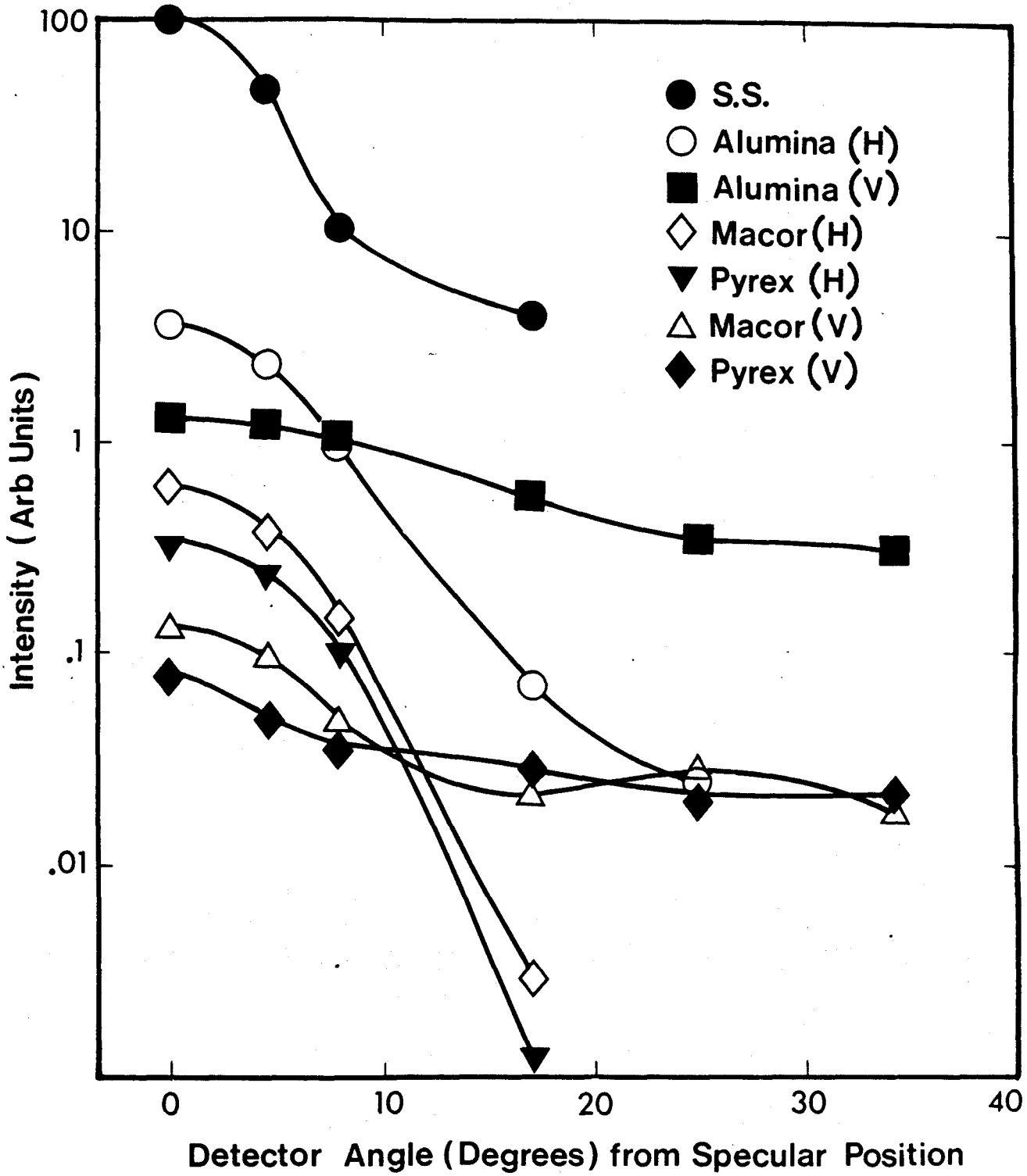
100
10
1
.1
.01
Intensity (Arb Units)
0
10
20
30
40
Detector Angle (Degrees) from Specular Position
S.S.
Alumina (H)
Alumina (V)
Macor (H)
Pyrex (H)
Macor (V)
Pyrex (V)

Figure 5.

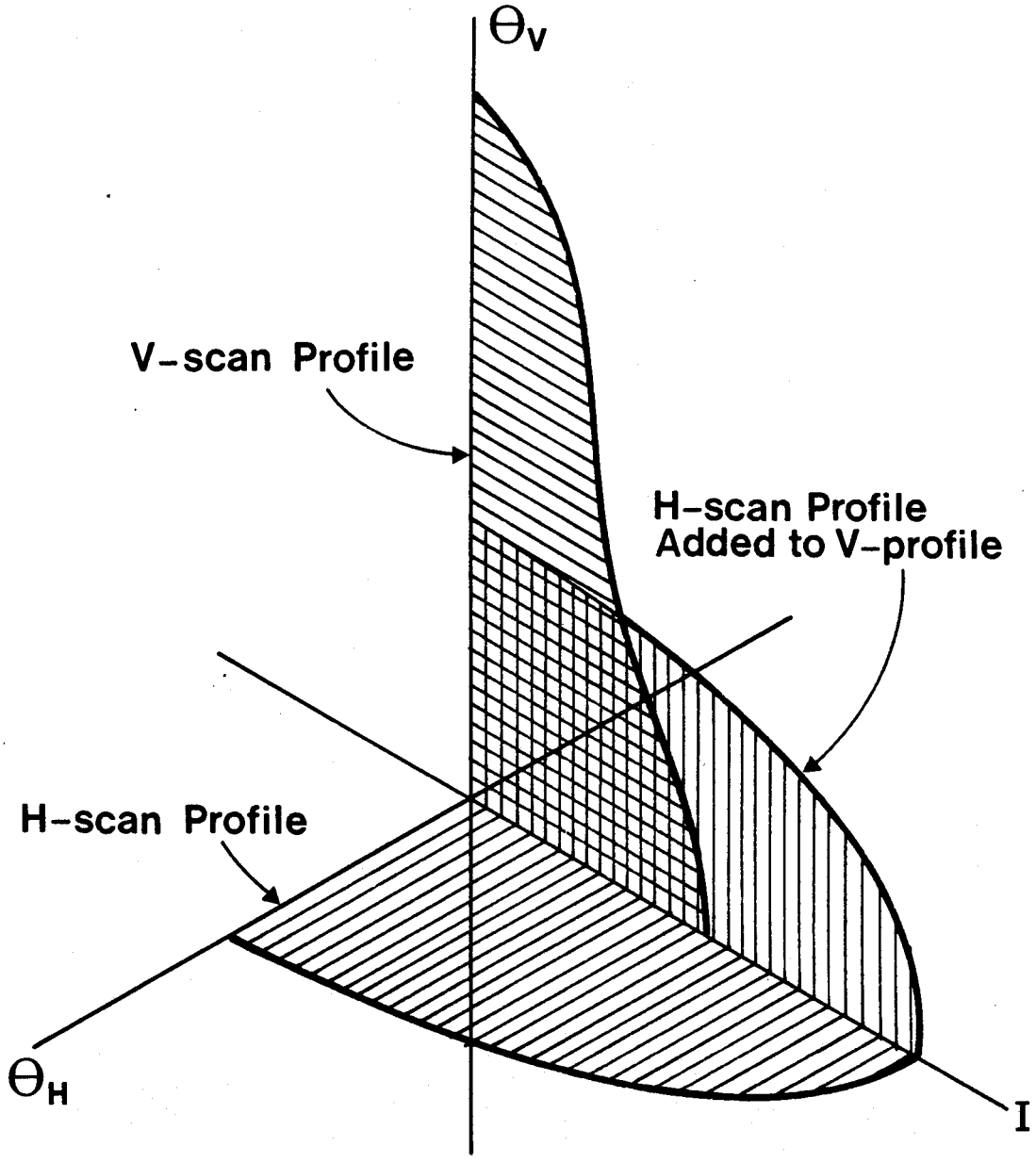
Θ_V
V-scan Profile
H-scan Profile
Added to V-profile
H-scan Profile
Θ_H
I

Figure 6.

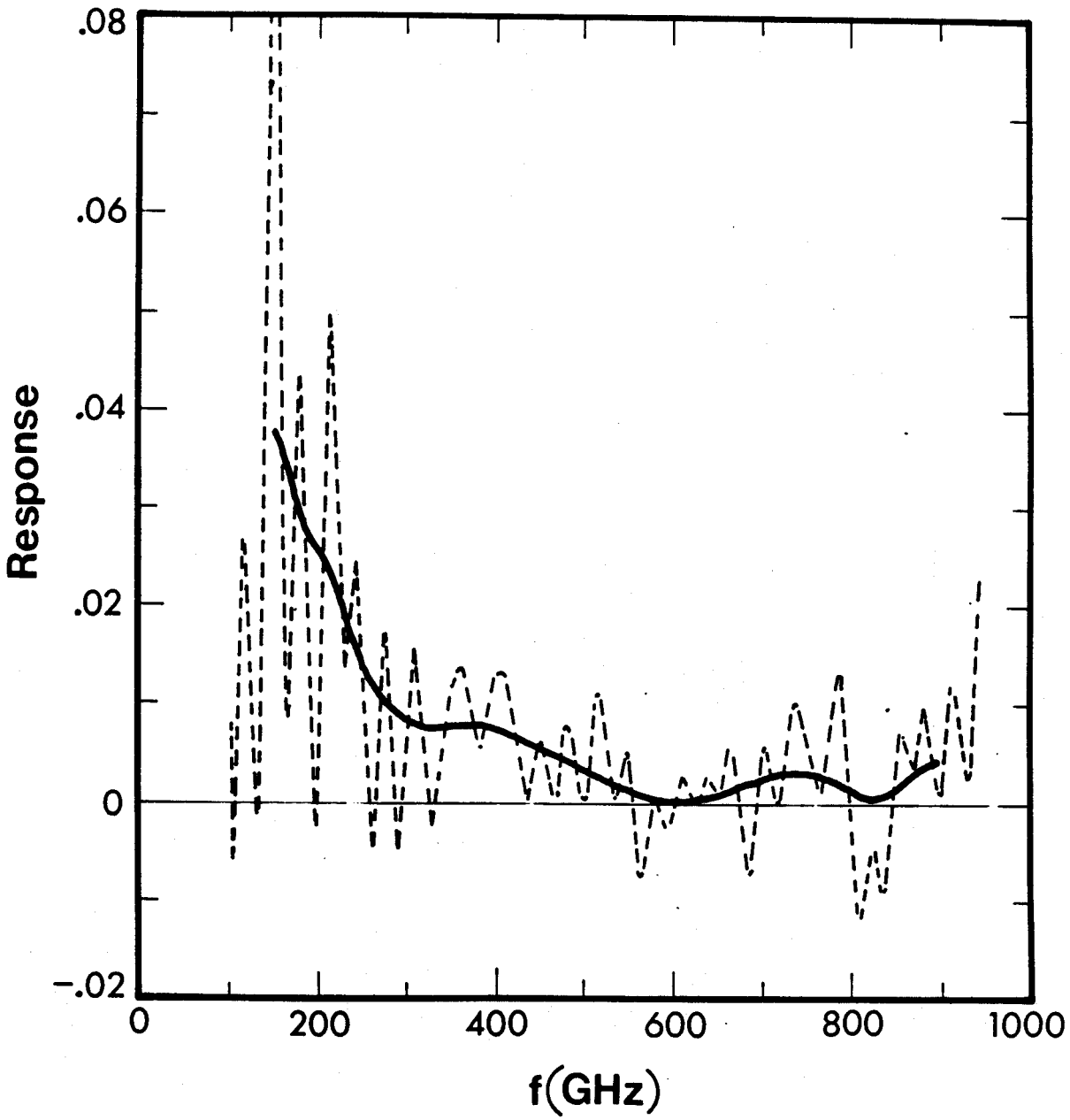

Figure 7.

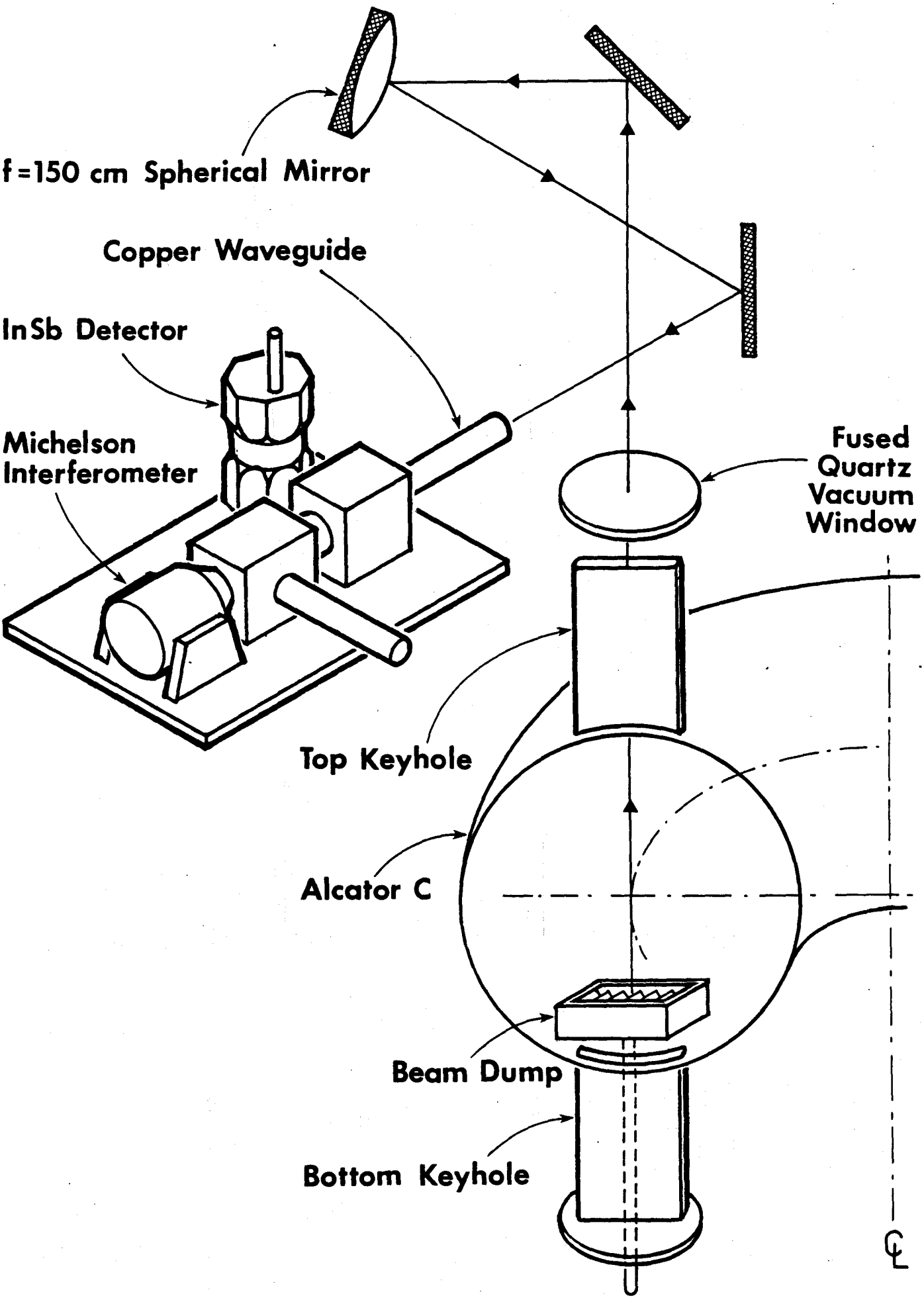
f=150 cm Spherical Mirror
Copper Waveguide
InSb Detector
Michelson Interferometer
Fused Quartz Vacuum Window
Top Keyhole
Alcator C
Beam Dump
Bottom Keyhole
℄

Figure 8.

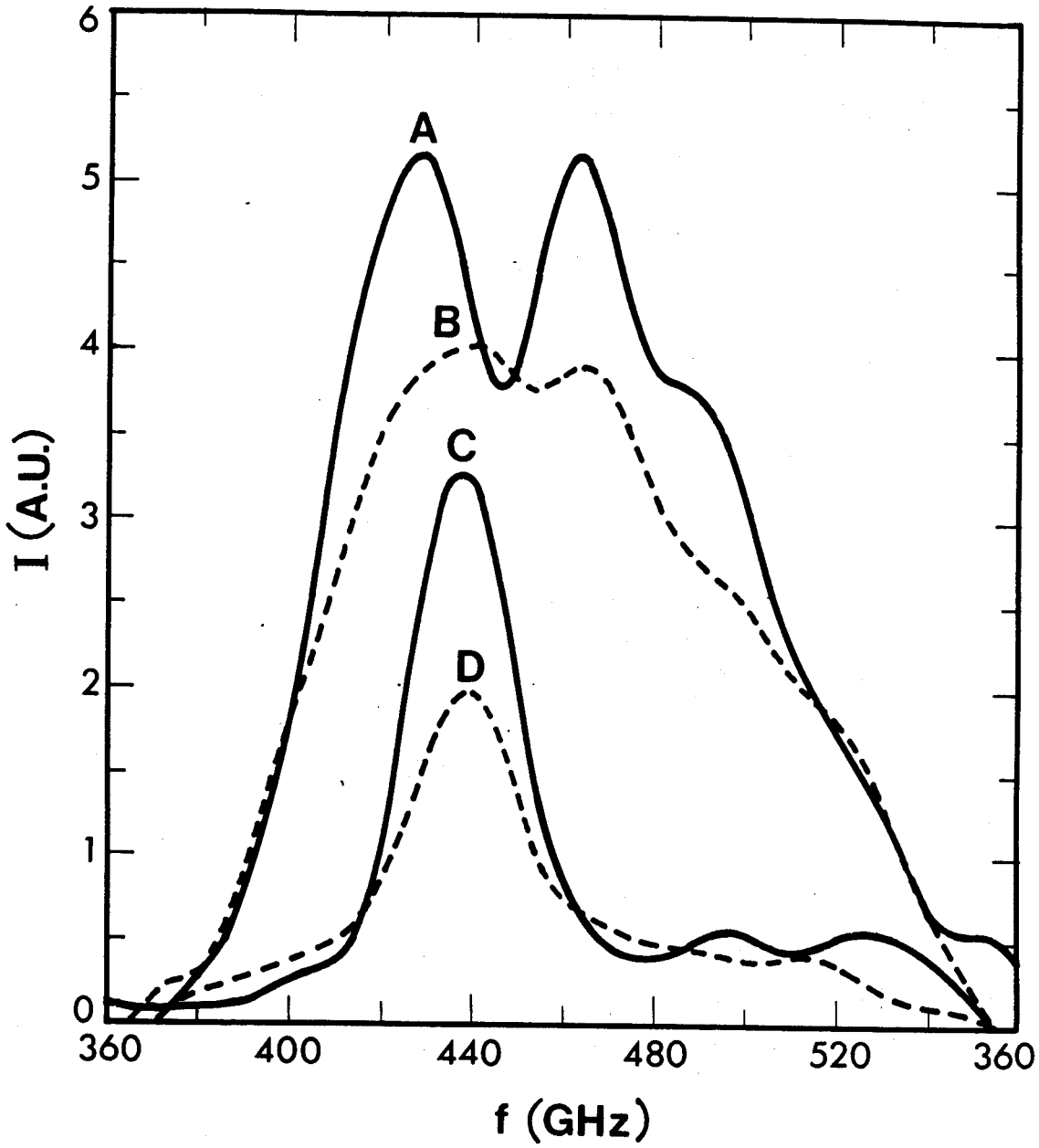

Figure 9.